PHILOSOPHICAL TRANSACTIONS OF THE ROYAL SOCIETY A

Phil. Trans. R. Soc. A (2012) **370**, 3241–3268
doi:10.1098/rsta.2012.0104

Review

Solar flares and energetic particles

By Nicole Vilmer*

LESIA, Observatoire de Paris, CNRS, UPMC, Université Paris-Diderot, 5 place Jules Janssen, 92195 Meudon, France

Solar flares are now observed at all wavelengths from γ-rays to decametre radio waves. They are commonly associated with efficient production of energetic particles at all energies. These particles play a major role in the active Sun because they contain a large amount of the energy released during flares. Energetic electrons and ions interact with the solar atmosphere and produce high-energy X-rays and γ-rays. Energetic particles can also escape to the corona and interplanetary medium, produce radio emissions (electrons) and may eventually reach the Earth's orbit. I shall review here the available information on energetic particles provided by X-ray/γ-ray observations, with particular emphasis on the results obtained recently by the mission Reuven Ramaty High-Energy Solar Spectroscopic Imager. I shall also illustrate how radio observations contribute to our understanding of the electron acceleration sites and to our knowledge on the origin and propagation of energetic particles in the interplanetary medium. I shall finally briefly review some recent progress in the theories of particle acceleration in solar flares and comment on the still challenging issue of connecting particle acceleration processes to the topology of the complex magnetic structures present in the corona.

Keywords: Sun; flares; X-rays; γ-rays; radio bursts; solar energetic protons

1. Introduction

Solar flare observations started in 1859, when Carrington [1] observed in white light a localized brightening of the solar surface lasting a few minutes. Since then, local brightening (flaring) of the Sun has been observed at many wavelengths both from the ground and from space. The basic picture of a flare was established in the 1980s (e.g. [2]). Solar flares are linked to sudden explosive release of the free magnetic energy contained in current-carrying ('non-potential') magnetic fields. The release of the free magnetic energy can proceed through the process of magnetic reconnection, when changes of the connectivity of the magnetic field occur. There is increasing observational evidence supporting that magnetic reconnection and subsequent large-scale reconfiguration play a major role in the rapid transformation of stored magnetic energy in a flare. It is however far less clear how a large fraction of the magnetic energy can be converted to non-thermal

*nicole.vilmer@obspm.fr

One contribution of 11 to a Theme Issue 'Astrophysical processes on the Sun'.

particles. The Sun is indeed a powerful particle accelerator. This has been known for years, since the first detection of solar energetic protons by ground-based neutron monitors, the first detection of solar flares in radio and X-rays, the first observations of γ-ray line flares from energetic protons in 1972 and first detection of more than 100 MeV solar neutrons aboard SMM/GRS in 1982 (see for a recent review, see [3]).

Solar flares and coronal mass ejections (CMEs) are the most powerful events in the solar system. In several tens of minutes, they can convert up to 10^{32} ergs of magnetic energy into accelerated particles, heated plasma and ejected solar material. Recent estimates of the energy budget have been achieved for two events [37] based on a comprehensive study of many observations (ACE, RHESSI, SOHO, TRACE, WIND, GOES) (for a review, see [5]). It was shown that for the 23 July 2002 γ-ray line flare observed by RHESSI, the energy contained in energetic electrons interacting at the Sun was comparable to the energy contained in interacting ions and comparable to the CME energy. Understanding particle acceleration is thus one crucial element of the study of solar flares.

2. Hard X-ray and γ-ray diagnostics of flare energetic particles

The most quantitative diagnostics of energetic particles interacting at the Sun come from hard X-ray/γ-ray observations, which provide information on electron and ion energy spectra, numbers and energy contents. Figure 1*a* shows a theoretical HXR/GR spectrum of a solar flare from 1 keV to 100 MeV. Flare-accelerated electrons (energies more than 10 keV) produce bremsstrahlung continuum emission by their braking in the Coulomb field of ambient ions, and above 500–700 keV of ambient electrons [8] (for recent reviews, see [9,10]). This continuum (curves 3 and 5) is dominant below 1 MeV and again in the 10–50 MeV range. Energetic ions with energies in the more than 1 MeV per nuc to 100 MeV per nuc range produce, through interactions in the solar atmosphere, a complete γ-ray line spectrum (curve 4), which consists of several nuclear de-excitation lines, neutron capture and positron annihilation lines (for reviews, see [11–13]). When ions over a few hundred MeV per nuc are produced in the flare, nuclear interactions with the ambient medium produce secondary pions whose decay produces a broadband continuum at photon energies above 10 MeV (with a broad peak around 70 MeV from neutral pion radiation; curve 6) and also secondary neutrons which, if energetic enough, may escape from the Sun and be directly detected in interplanetary space or at ground level (respectively, more than 10 MeV or 200 MeV neutrons; for a review, see [14]).

The temporal and spectral characteristics of HXR/GR continua and γ-ray line emissions provide quantitative information on acceleration time scales (less than 100 ms for electrons; less than 2 s for ions), electron and ion energy spectra, numbers as well as energetic ion abundances. Figure 1*b* shows an example of the temporal evolution of HXR and GR line emissions observed by RHESSI for the 23 July 2002 flare. The 2.223 MeV line from neutron capture radiation is as expected delayed by $\simeq$100 s with respect to the prompt γ-ray lines in the 2.2–7 MeV range. This is due to the time needed for the thermalization of the

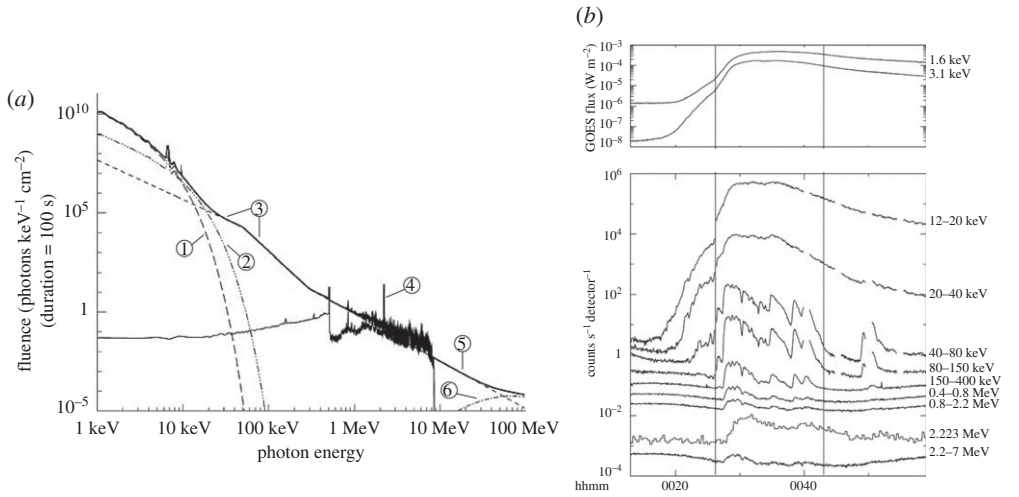

Figure 1. (*a*) Composite X-ray/γ-ray spectrum from 1 keV to 100 MeV for a large flare. At energies up to ≃10–30 keV, emission from hot (≃ 10^7 K; curve 1) and superhot (≃ 3×10^7 K; curve 2) thermal flare plasmas. Bremsstrahlung emission from energetic electrons produces the X-ray/γ-ray continuum (curves 3 and 5) up to tens of MeV. Broad and narrow γ-ray lines from nuclear interactions of energetic ions sometimes dominate the spectrum between ≃1 and 7 MeV (curve 4). Above 70 MeV, the photons produced by the decay of neutral pions (curve 6) sometimes dominate (adapted from [6]). (*b*) RHESSI HXR and γ-ray count rates for the 23 July 2002 flare, scaled to fit: 20–40 keV × 0.3; 40–80 keV × 0.07; 80–150 keV × 0.02; 150–400 keV; 400–800 keV × 0.001; 800–2218 keV × 0.0005; 2218–2228 keV × 0.01; and 2228–7000 keV × 2 × 10^{-5}. The slow variation through the interval is due to background counts from cosmic ray interactions with the atmosphere and spacecraft (from Lin *et al.* [7]).

fast neutrons produced in the nuclear reactions, before they can be captured by ambient hydrogen, to produce deuterium in an excited nuclear state leading to the emission of a 2.223 MeV photon.

High-energy observations of solar flares have been observed for three solar cycles. Before the launch of the solar dedicated RHESSI mission [6], emission above 100 keV was one of the last domains where no spatially resolved observations were obtained. Before the launch of RHESSI and of INTEGRAL in 2002 [15], quantitative information derived on energetic electrons and ions from HXR/GR spectroscopy had been deduced from observations with limited spectral resolution. Since then, several flares have been observed in the hard X-ray domain at a high spectral resolution with RHESSI and several γ-ray flares have been observed with both RHESSI and INTEGRAL for which a detailed γ-ray line shape analysis has been achieved.

3. Energy release and particle acceleration sites

(*a*) *Particle interaction sites and magnetic environment*

Solar flares usually occur in magnetic active regions. Flares were originally observed in the Hα line originating in the chromosphere. Hα flare brightenings

(ribbons) are usually elongated features lying on either side of a magnetic polarity inversion line (figure 2). The largest flares occur in large active regions showing complex magnetic field geometries. The magnetic reconfiguration that allows the rapid release of stored magnetic energy in flares is believed to occur somewhere above the chromosphere in the low corona (see the reconnection region in figure 3). Flare Hα ribbons are related to the magnetic topology in which the flare occurs; they trace the projection of the separatrix or quasi-separatrix structures which indicate changes of magnetic connectivity in the active region (e.g. [19]). While the HXR footpoints (figures 2 and 3) result from the direct impact of non-thermal electrons in the solar chromosphere, the flare ribbons observed in Hα or in UV reveal excitation owing to thermal conduction from the hot plasma or from weak particle precipitation. In Hα and EUV, the flare ribbons have a tendency to spread systematically outwards from the magnetic polarity inversion line as the flare progresses. Such observations support the standard magnetic reconnection model (figure 3*a*). On the other hand, HXR footpoints are found at specific locations of the flare ribbons and usually in small numbers (most commonly two to three at a given time; figure 2). The HXR footpoint sources frequently move along the Hα or UV/EUV ribbons rather than away from the polarity line. This was demonstrated in, for example, Bogachev *et al.* [18] who systematically analysed HXR footpoint motions for 72 flares of the YOHKOH/HXT (Hard X-ray Telescope) database. Only around 10 per cent of the flares show footpoint motions away from and nearly perpendicular to the neutral line as would be expected if the reconnection site moves higher in the atmosphere as the flare progresses (figure 3*a*). For 26 per cent of the flares, the footpoints move in anti-parallel directions to the neutral line (such as shown in figure 3*b*), suggesting that the field lines are highly sheared. In an even higher number of flares (35%), footpoint motions are found to be parallel along the neutral lines and in 26 per cent of flares even more complicated footpoint motions are observed. Many individual examples observed either with YOHKOH/HXT or with RHESSI confirm that the HXR footpoint motions do not always agree with the 'standard model' predictions of separating footpoints (for a review, see [5]). Figure 4*a* shows the YOHKOH HXR source motions compared with the projections of the magnetic separatrices as reported by Metcalf *et al.* [20]. For another event observed by RHESSI, des Jardins *et al.* [21] showed that the path of the HXR footpoints is along some spine lines (i.e. lines joining two magnetic sources of the same sign via a null point; figure 4*b*). If recent years have seen great advances in understanding the topology of the complex magnetic field in the active region and in analysing separatrix and quasi-separatrix layers, magnetic null points, etc. (e.g. [22]), then the location of the HXR footpoints and their motions with respect to flare ribbons and magnetic topology in general still largely remains an open question. This topic will remain in the next few years an area of intense activity.

(*b*) *Electron acceleration sites and current sheets*

As recalled earlier, HXR (more than 20 keV) images usually show double compact sources (figure 2 and sources (F) in figure 5). They are interpreted as the footpoints of magnetic loops in which electrons propagate from the acceleration site before they impinge on the chromosphere and produce thick-target X-ray emission. Typical heights where electrons of tens to a few hundreds of keV

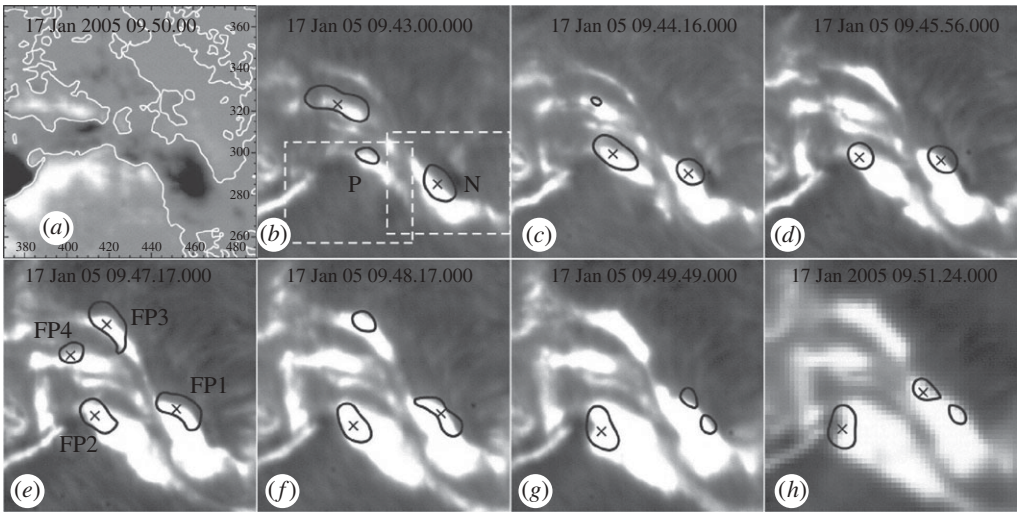

Figure 2. (*a*) Longitudinal photospheric magnetic field measured by SOHO/MDI. The white lines indicate the magnetic inversion lines. (*b–h*) The evolution of the Hα flare ribbons (Hα filtergrams in *b–g* and Hα −0.3 Å filtergrams in *h*). The 40% contours of the closest-in-time RHESSI 30–100 keV HXR image together with the source centroids (crosses) are overlaid (from Temmer *et al.* [16]).

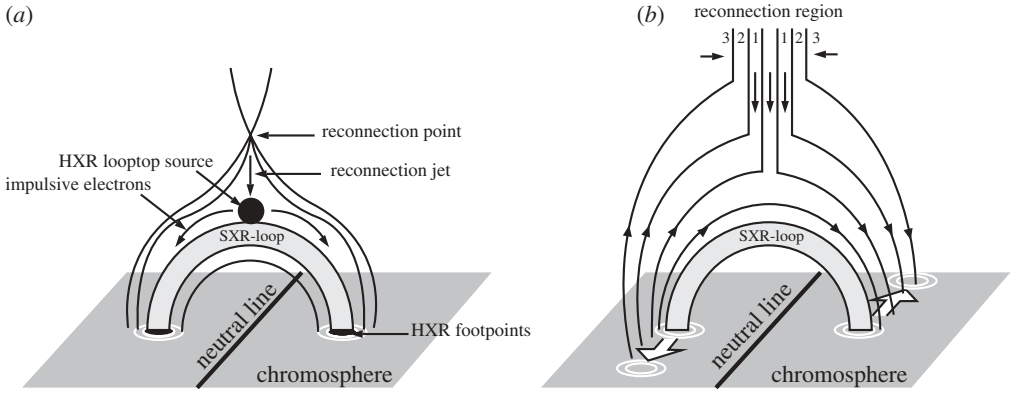

Figure 3. (*a*) Scenario for magnetic reconnection, particle acceleration and radiation emitting sites in solar flares (adapted from [17]). (*b*) Evolution of the magnetic line reconnection (1–2–3) in a highly sheared magnetic configuration and associated HXR source motions (adapted from Bogachev *et al.* [18]).

are accelerated have been estimated from time of flight analysis of hard X-ray emissions leading to estimates of the acceleration heights ranging between 2×10^4 and 5×10^4 km [24]. This estimation of electron acceleration heights is based on the thick target model of X-ray emission introduced by Brown [8], which is now known to require substantial modifications owing to theoretical difficulties such as beam stability [25]. Energy-dependent delays of HXR pulses could then be attributed not only to time of flight effects but also to evolution (softening) of the

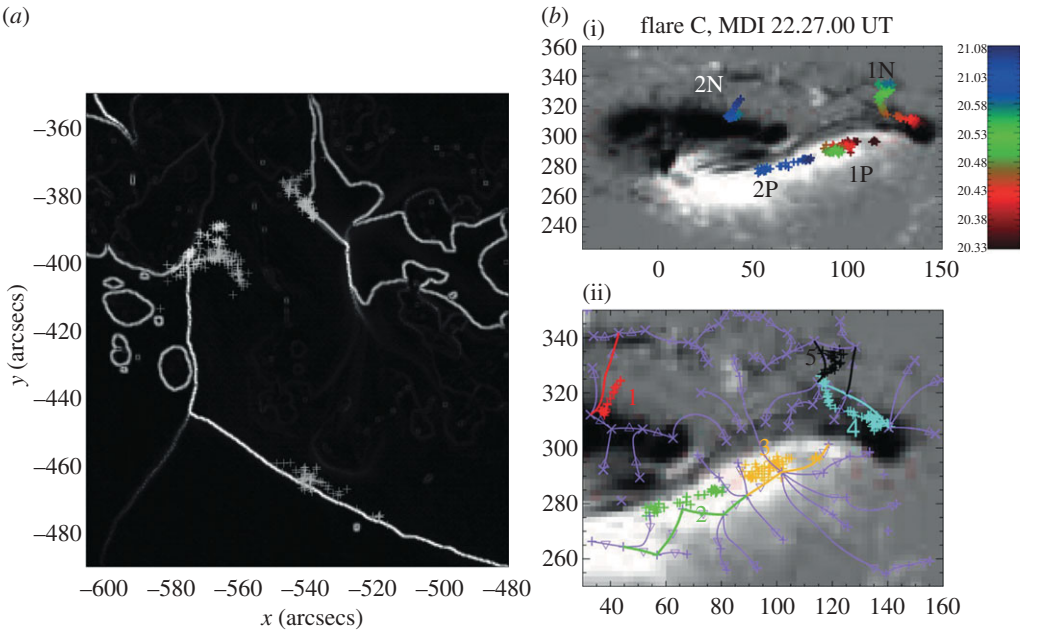

Figure 4. (*a*) The location of HXR footpoints at different times in the flare of 25 August 2001, with respect to the magnetic separatrices computed from a potential field model of the active region. The plus signs show the location of the HXRs, and the lines show the separatrices. The brightness of the separatrix indicates the magnitude of the discontinuity (from Metcalf *et al.* [20]). (*b*) (i) SOHO/MDI line-of-sight magnetic field image and RHESSI HXR footpoint tracks (the colour-coded UT time scale is shown to the right). Each plus symbol marks the centroid location of a source at 25–300 keV. The centroids are plotted every 20 s from 22.32.40 to 23.08.20. (ii) Poles, nulls, spine lines and HXR footpoint tracks on magnetograms. Violet lines are spine lines not associated with HXR footpoints. Spine lines marked with non-violet colours were identified with the HXR footpoint tracks of similar colour (adapted from des Jardins *et al.* [21]).

spectrum of electrons injected in the target [26]. Although only double compact sources or footpoints are observed in most events, occasionally additional compact loop-top sources are observed in some events (figure 5). The compact loop-top sources (LT) at higher X-ray energies are found to be located at higher altitudes and have been interpreted as the result of the energization of the plasma by shocks originating from the reconnection site in the low corona (figure 3). The existence in images of HXR footpoints and of loop-top sources brings support to the simple time of flight model of Aschwanden *et al.* [24] and to a location of the acceleration region in the corona [26]. In addition to loop-top sources, coronal (C) sources have also been observed with RHESSI at energies up to 16 keV (figure 5). While the temperature of the loop-top sources increases with increasing altitudes, the temperature of the coronal sources increases with decreasing altitudes. These observations may indicate the existence between the loop-top and coronal sources of a current sheet in which magnetic energy conversion takes place. This is further supported by the EUV observation for one event of high-speed and high-temperature plasma flows near the location of the current sheet. These are interpreted as reconnection outflows [27]. Few events with loop-top and coronal

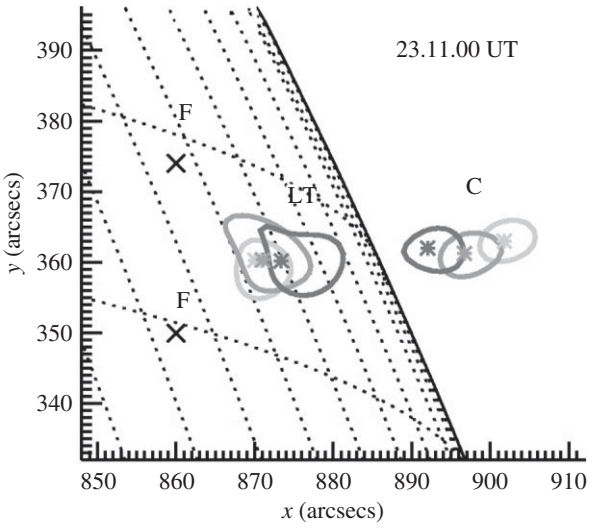

Figure 5. RHESSI images observed in different energy bands. Loop top (LT) sources in the following energy bands: 6–8, 10–12 and 16–20 keV (from light to dark contours) are shown. The contours of the coronal sources (C) above the limb are light to dark, respectively, for the 10–12, 12–14 and 14–16 keV energy bands. The crosses mark the two footpoints (F) of the X-ray loop (from Sui & Holman [23]).

sources (less than 5) have however been observed so far (see the review by Fletcher *et al.* [5]), and it is one of the goals of future hard X-ray imagers with higher dynamic ranges to confirm, using more events, the existence of these loop-top and coronal sources so as to provide a stronger support to the idea that electrons are accelerated in such current sheets.

(*c*) *High coronal sources*

Although the most intense flare emissions are observed from the chromospheric footpoints (see §3*b*), there are, however, several observations of hard X-ray and even γ-ray emission directly from the corona. It is particularly interesting to study the coronal sources because they occur close to the presumed particle acceleration sites. Prior to RHESSI images, most of the non-thermal coronal sources had been studied using disc occultation (for a review, see [28]). One of the most impressive observations of coronal sources with RHESSI is provided by the observations of the 20 January 2005 event for which coronal emission was observed above 500 keV [29]. Figure 6 shows that while the footpoint emission dominates during the γ-ray peak, the coronal source becomes more and more prominent as the flare decays and is observed even at energies above 500 keV. The imaging-spectroscopic capability of RHESSI, furthermore, allows the photon spectrum from the corona and from the footpoints to be measured (figure 7*a*). The coronal source is found to have a much flatter (harder) spectrum (with a power-law index between −1.5 and −2) than the footpoints (power-law index between −3 and −4). Fits to the complete γ-ray spectrum reveal that most of the emission in the 525–830 keV range is due to relativistic electron bremsstrahlung and not to γ-ray lines [29]. The coronal source in the 525–830 keV range is then produced through bremsstrahlung

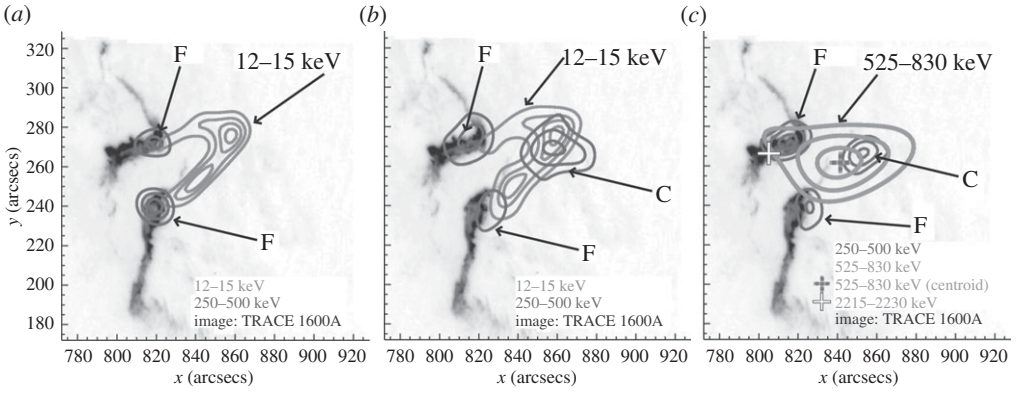

Figure 6. Imaging of the 20 January 2005 flare. (*a*) During the γ-ray peak (06.43.32–06.46.40 UT). (*b*) During the end of the decay phase (06.49.30–06.55.01 UT). (*c*) Averaged over the decay phase (06.46.44–06.55.01 UT). All figures show a TRACE 1600 Å image taken at 06.45.11 UT. (*a*,*b*) Contours (in light grey) of thermal flare emission at 12–15 keV and contours (dark grey) of non-thermal emission at 250–500 keV for the foot points (F) and for the coronal source (C). (*c*) Contours (light grey) of the source at 525–830 keV with a spatial resolution of 37 arcsecs full width at half maximum and contours (dark grey) of the sources at 250–500 keV. The centroids of the sources in the 525–830 keV range (dark grey cross) and for the 2.2 MeV line (white cross) are also shown (adapted from Krucker *et al.* [29]).

of relativistic electrons with an extremely hard spectrum. Previous observations (with no direct imaging information) of partially occulted large flares with coronal emissions up to the γ-ray range [31–34] also exhibit very hard photon spectra up to very high energies (see figure 7*c*). If the coronal source is representative of the electron spectrum in the acceleration region, it is worth noting that such a flat spectrum is expected from the acceleration scenarios in which multiple acceleration sites are considered (see §7).

(*d*) *Electron and ion interaction sites*

One of the most intriguing results from RHESSI imaging comes from the observations of the first γ-ray line event ever imaged (figure 8*a*). The 2.2 MeV neutron capture line location was displaced by 20″ from the centroid of the HXR sources in the 50–100 keV range imaged in the same conditions [35]. Although the 2.2 MeV line images the neutron interaction site rather than the energetic ion interaction site itself, it was nevertheless shown that the 2.2 MeV line emission locates the energetic ion interaction region within 1″, thus still implying a previously unexpected significant displacement between the ion and electron interaction sites. Imaging in the γ-ray line domain with RHESSI has been achieved now for five events (see [35,36], and figure 8 illustrating a few of these events). For four of the five events, a single unresolved source is observed in the γ-ray line domain but, given the constraints of the imaging technique, there is no evidence that the true γ-ray line sources are predominantly single sources. Statistically significant displacements between HXR and γ-ray line sources were observed in three of the five events. Given the limited number of observations, it is still difficult to draw firm conclusions on the relative locations

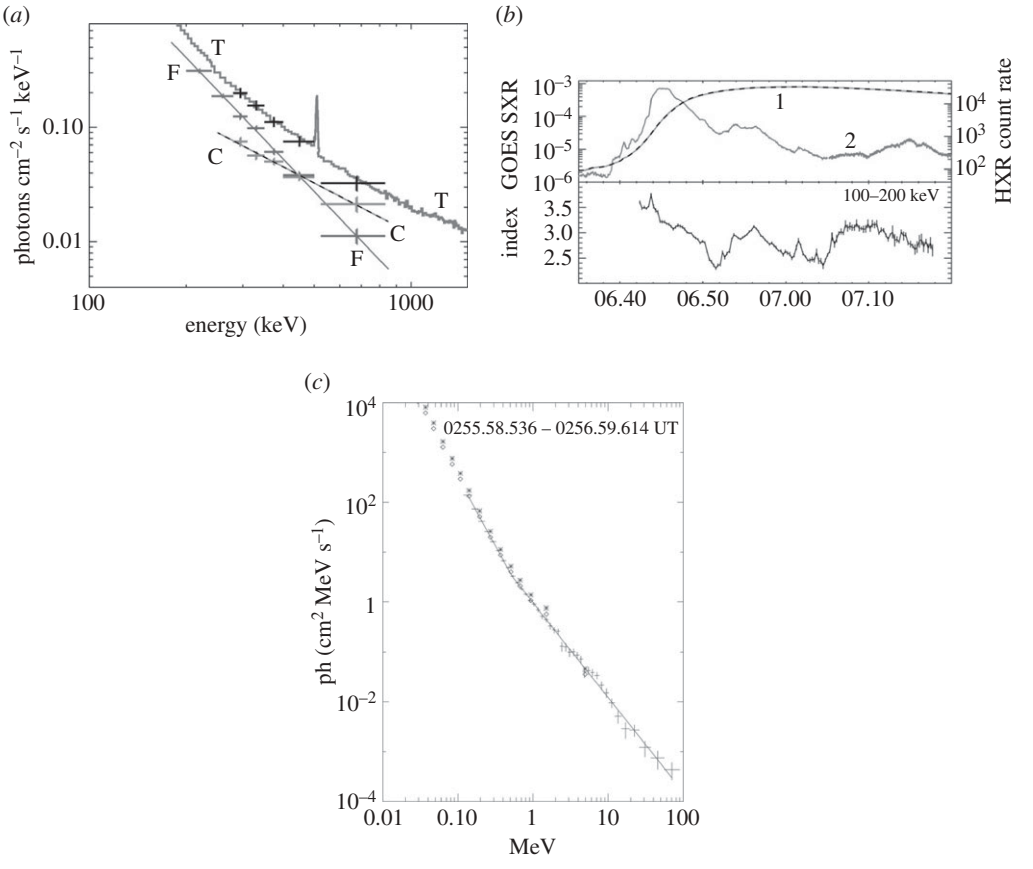

Figure 7. (*a*) Imaging spectroscopy with RHESSI of the 20 January 2005 flare for the time period corresponding to the image in figure 6*b*. The spectrum of the coronal source and the combined footpoint sources are indicated by C and F, respectively, and their sum is indicated by T. The power-law fits shown give a much harder spectrum for the coronal source (-1.5 ± 0.2) than for the footpoints (-2.9 ± 0.1). The higher spectral resolution but spatially integrated spectrum is also shown in plain line (from Krucker *et al.* [29]). (*b*) HXR spectral evolution for the 20 January 2005 flare. The GOES SXR (curve 1; low-energy channel) and RHESSI 50–100 keV HXR (curve 2) time profiles are shown in the top panel. The temporal evolution of the power-law index in the 100–200 keV energy band is presented in the bottom panel (adapted from Saldanha *et al.* [30]). (*c*) HXR/GR photon spectrum observed by PHEBUS/GRANAT for the occulted flare of 30 June 1991. The solid curve represents the best fit double power-law photon spectrum. The stars represent the photon spectrum deduced from the spectral analysis of BATSE count rates in the same time interval. The diamonds represent the same quantities divided by 1.3. The slope above 500 keV is −1.9 (from Vilmer *et al.* [31]).

of electron and ion interaction sites in many flares (for a review, see [13]). Improving the imaging in the γ-ray line domain is clearly one of the goals of future instruments.

The explanations of these displacements (clearly *not* instrumental) are still largely unknown even if several interpretations have been put forward. Emslie *et al.* [37] proposed an interpretation in terms of a stochastic acceleration mechanism in which ions are preferentially accelerated in larger loops than

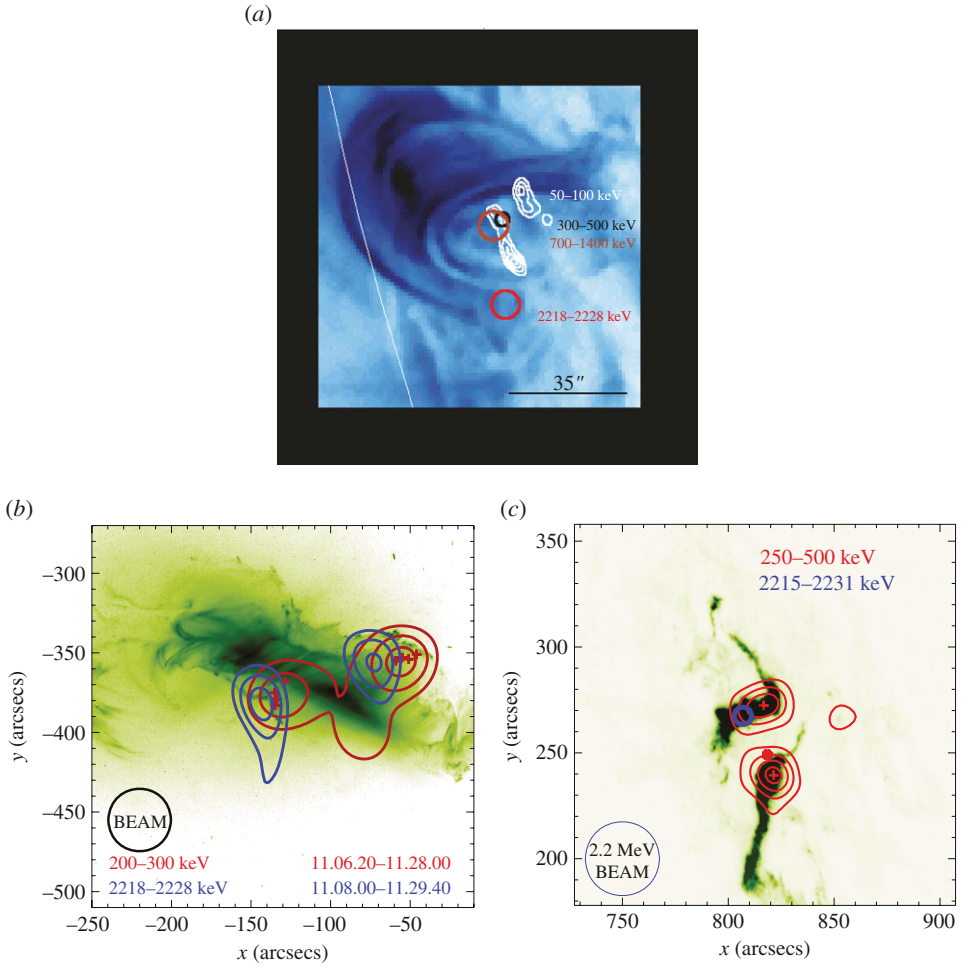

Figure 8. Respective location of γ-ray source at 2.223 MeV and of hard X-ray sources observed with RHESSI for different flares. (*a*) The 23 July 2002 event; the circles represent the 1σ errors for the 300–500 keV (black), 700–1400 keV (red) and 2218–2228 keV (pink) maps made with identical parameters. The white contours show the high resolution 50–100 keV map with 3″ resolution. The background is a TRACE image showing the post-flare loops (adapted from Hurford *et al.* [35]). (*b*) The 28 October 2003 event; RHESSI contours at 50%, 70%, and 90% (35″ resolution images) overlaid on a TRACE image (adapted from Hurford *et al.* [36]). (*c*) The 20 January 2005 event; contours of the 250–500 keV emission overlaid on a TRACE image and centroids (in red and blue) of the map performed in the 250–500 and 2215–2231 keV range (adapted from Vilmer *et al.* [13]).

electrons. The images for the 23 July 2002 event (figure 8*a*) would support such an interpretation of ions being injected in longer loops. For the same flare, the interpretation of time delays between γ-ray lines and hard X-rays in the framework of trap plus precipitation models [38] also supports the fact that ions are injected in longer loops than electrons. However, such an explanation is not appropriate for the 28 October 2003 event, where the footpoint separations for the electrons and ions are similar. Gradient and curvature drifts have been considered by Hurford *et al.* [36] to explain displacements, but the predicted

displacements between the ion and electron emitting sources are two orders of magnitude too small. Another possibility raised by Litvinenko & Somov [39] is that electric-field acceleration would lead to separation of particles with opposite charge (see also [40]).

4. Constraints on energetic electrons and ions deduced from high-resolution X-ray/γ-ray spectrum

(a) *Electron energy spectra and numbers in flares*

HXR/GR observations obtained with a high spectral resolution, such as those now achievable with RHESSI and INTEGRAL, enable a detailed analysis of the bremsstrahlung continuum and resolution of individual γ-ray lines. In the HXR domain, bremsstrahlung photon spectra at high resolution can be directly inverted to get the effective mean electron flux spectrum in the source [41]. Figure 9*a* shows for one event the comparison of the electron flux spectrum deduced by forward fitting of a model electron spectrum to the observed photon one and of the electron spectrum obtained through direct inversion. Electron spectra obtained through direct inversions are still rare (less than 10 events; for a review, see [10]). However, they bring crucial information for the understanding of electron acceleration because the electron flux spectrum deduced from the inversion is the quantity that must be compared with the predictions of acceleration models. In the most simple case, it represents the electron spectrum, with an isotropic pitch angle distribution, that would be required to produce the observed photon spectrum in a homogeneous source, under the most commonly used assumptions in X-ray models (X-ray emission primarily produced by bremsstrahlung radiation, no contribution from Compton back-scattered photons). However, if taken into account, anisotropies in the pitch angle distribution of energetic electrons could significantly alter the X-ray spectrum and modify the shape of the electron spectrum deduced through inversion [44] (for a review on the inversion of HXR photon spectra, see [10]).

Prior to the RHESSI launch, a lot of information had been obtained from numerous observations with limited spectral resolution, from the HXR spectra, the related electron spectra and from the number of energetic electrons needed to reproduce HXR bursts (see [45] for statistical observations of flares and [46,47] for reviews on the constraints on energetic electrons derived from HXR observations). For a large HXR (e.g. GOES X-class) flare, the required rate of acceleration of electrons above 20 keV can exceed 10^{37} electrons per second. For a flare lasting several minutes, this amounts to 10^{39} electrons, which represents the acceleration of electrons from a very large volume in the corona. For many years, this has been known as the number problem. The spectral index in the HXR domain varies in the course of the event and from flare to flare but remains most of the time in the (−2,−6) range. In most powerful flares, the photon spectra may reveal double power laws below 300 keV, with the spectral index from below 30 to 60 keV being smaller (flatter) than that above 60 keV by two to four units [48]. For the most energetic flares, emission from relativistic and ultrarelativistic electrons can be observed up to a few hundred MeV (for reviews, see [13,14]). At photon energies more than 500 keV, arising from electrons of higher energies, the

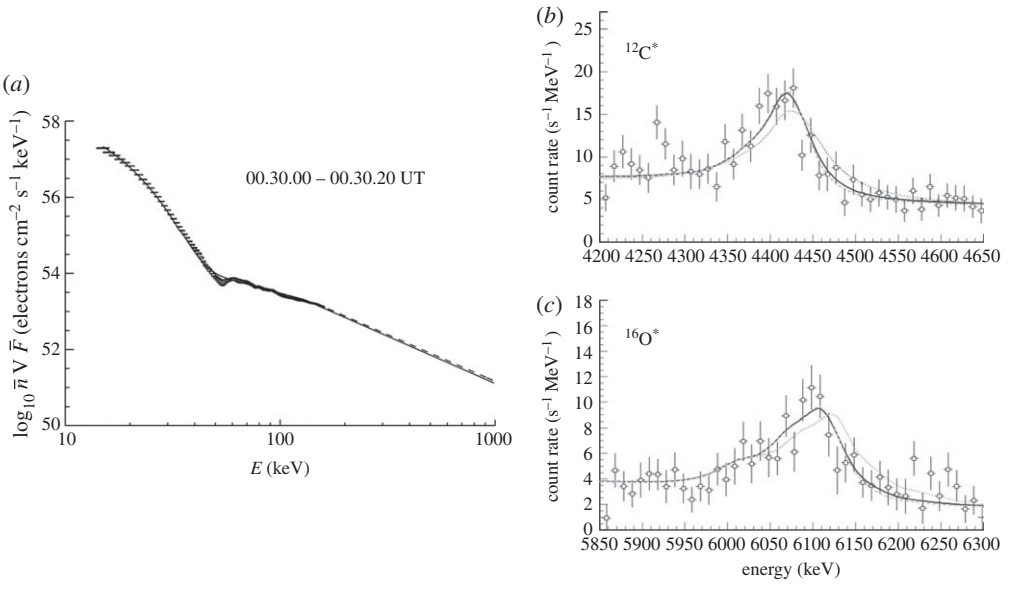

Figure 9. (*a*) Regularized mean electron flux spectrum obtained from the inversion of the photon spectrum (data points) observed by RHESSI [41]. The solid line shows the forward fitted electron spectrum necessary to reproduce the same X-ray spectrum [42]. (*b*,*c*) Observed and calculated line shapes of the 4.44 and 6.13 MeV ambient ^{12}C and ^{16}O de-excitation lines observed by INTEGRAL/SPI for the 28 October 2003. The dark line represents the calculated line shape for a downward isotropic distribution. The dotted line represents the calculated line shapes for another model (see [43] for details; from Kiener *et al.* [43]).

spectrum tends to flatten again. Such a flattening (not the one attributed to pion decay radiation which arises at much higher energies) has been observed in a few events with PHEBUS/GRANAT. It can be as large as 1.5–2 units at energies from 600 keV to several tens of MeV [31,49]. This is a much larger flattening than the one expected from the contribution of electron–electron bremsstrahlung (figure 7*c*). It is attributed to a flattening (hardening) of the energetic electron spectra at energies above 500 keV. All the characteristics of energetic electron spectra derived from the observations should be ideally explained by electron acceleration models.

(*b*) *Ion energy spectra, numbers and abundances in flares*

Interactions of energetic ions in the energy range from more than 1 MeV nuc^{-1} to 100 MeV nuc^{-1} produce an extensive spectrum of γ-ray line emission. Narrow γ-ray lines result from the bombardment of the ambient nuclei by accelerated protons and α-particles, whereas broad lines occur from the inverse reactions, in which accelerated heavy nuclei collide with ambient hydrogen or helium nuclei. De-excitation γ-ray line spectra provide information on flare ions of energies more than 1 MeV nuc^{-1}. The shape of the ion distribution below this energy is essentially unknown but is of particular interest for estimating the total energy content in ions. Several ratios of pairs of nuclear lines are used to infer the ion energy spectrum and energy content: the ratio of the flux in the 2.2 MeV

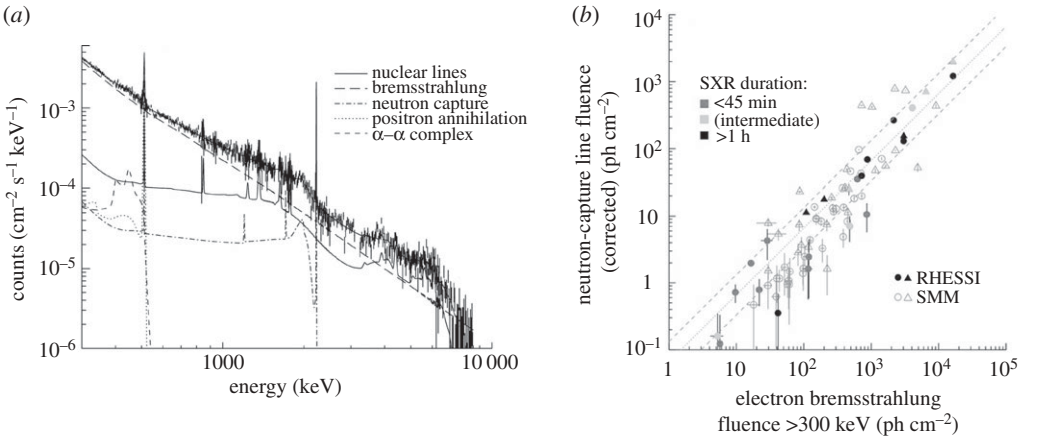

Figure 10. (*a*) RHESSI γ-ray count spectrum for the 23 July 2002 flare. The lines show the different components of the model used to fit the spectrum (from Lin *et al.* [7]). (*b*) Neutron capture line fluence as a function of the electron bremsstrahlung fluence above 300 keV for flares with heliocentric angle <80° (RHESSI in solid symbols, SMM in open symbols). Circles (triangles) represent flares with complete (incomplete) coverage. Light, middle and dark grey represent the SXR duration in three bins. The dotted line is the best fit in linear space that passes through the origin with a slope of 0.066 (from Shih *et al.* [53]).

line with respect to the flux in the prompt γ-ray lines in the 4–7 MeV range and the ratio of the fluxes from the de-excitation lines from neon and oxygen at 1.63 and 6.13 MeV [50,51]. The accelerated ion spectra are found to extend as unbroken power laws down to at least 2 MeV nuc^{-1} if a reasonable ambient Ne/O abundance ratio is assumed, i.e. in agreement with measurements of the Ne/O abundance ratio in the corona [52]. For the 19 SMM flares measured before the launch of RHESSI, the average spectral index was around −4.3; however, the events observed with RHESSI tend to have much harder (flatter) slopes [7,12]. Even though most of the energy contained in ions resides in protons and α-particles, the abundances of heavier accelerated ions also provide constraints for acceleration processes. Information on the abundances of flare-accelerated ions was deduced for the SMM/GRS flares, as well as for a few flares observed by RHESSI. A noticeable enhancement has been observed in the numbers of α-particles (up to 0.5 in some events), as well as of accelerated ^{3}He isotopes, compared with the standard coronal abundances. Furthermore, accelerated heavy ions, such as Ne, Mg and Fe, are also found to be over-abundant with respect to normal coronal compositions as reviewed in Vilmer *et al.* [13]. This poses other constraints on models for ion acceleration.

Spectral resolution provided by both the RHESSI (figure 10*a*) and the non-solar-dedicated INTEGRAL/SPI instrument (figure 9*b*,*c*) in the γ-ray line domain gives better measurements of the line fluences and permits analysis of the line shapes. This provides both information on proton and α-particle energy and angular distributions. Figure 9*b*,*c* shows an example of the γ-ray line shapes measured for a solar flare at high spectral resolution with INTEGRAL/SPI. The comparison of the results of detailed calculations of line shapes with the observations provides additional constraints on the ratio of accelerated helium

with respect to accelerated protons (α/p) in the flare [43]. The line shapes depend, however, on many parameters: angular distribution of interacting ions, spectral index of the energetic ions and α/p so that only the combination of line shapes and line fluences can provide information on regions of allowed parameters; in the case shown in the figure, this leads to the determination of the ion spectral index between −3 and −4, a relatively low value of α/p around 0.1 and a relatively wide angular distribution of emitting ions [43]. The number of flares for which γ-ray line spectra at high resolution have been obtained is still very small (around five combining RHESSI and INTEGRAL/SPI observations; for a review, see [13]), but this is a very promising field to deduce more constraints on the parameters of accelerated ions in flares.

(*c*) *Do all flares accelerate ions?*

Using the ion and electron spectra derived from γ-ray and X-ray spectroscopy, it is possible to compare the energies contained in flare-accelerated ions and electrons. Such an analysis based on 19 events from SMM/GRS [54] and a few events observed with RHESSI [37] shows that the energy contained in more than 1 MeV ions ranges from 10^{29} to 10^{32} ergs and is comparable to the energy contained in sub-relativistic electrons. However, there are large uncertainties in the determination of these quantities mostly attributed to the inaccurate determination of the low-energy end of the accelerated spectrum. The relative importance of electron and ion acceleration can also be addressed by comparing the production of ions and quasi-relativistic electrons (more than 300 keV) in flares. Such an analysis has been performed using both SMM/GRS [55,56] and RHESSI [53] observations. Good correlations are found (figure 10*b*) between the neutron-capture line fluence (taken as representative of the total energy content in protons above 30 MeV) and the bremsstrahlung fluence above 300 keV (taken as representative of the total energy content in electrons above 300 keV). This strongly suggests that high-energy electrons (above 300 keV) and ions are linked through a common acceleration process. Some correlation between the proton number above 30 MeV, the electron number above 50 keV and the soft X-ray GOES class is also found from the statistical study of Shih *et al.* [53], but only above a certain threshold in the level of ion production. These observations suggest that the acceleration of protons is more related to the acceleration of high-energy electrons than to the acceleration of the more numerous sub-relativistic ones.

5. Radio diagnostics of flare-accelerated particles

(*a*) *Electron acceleration and propagation in the low corona from combined HXR and radio observations*

Complementary observations of the HXR bremsstrahlung emitting electrons are provided by the radio emission produced in the whole frequency range from 100 GHz to a few megahertz. More information on this topic can be found in reviews by, for example, Pick & Vilmer [57]. Radio emissions at metric/decimetric wavelengths (i.e. in the 100 MHz–1 GHz range) are most commonly produced by coherent plasma radiation mechanisms and are a sensitive diagnostic of

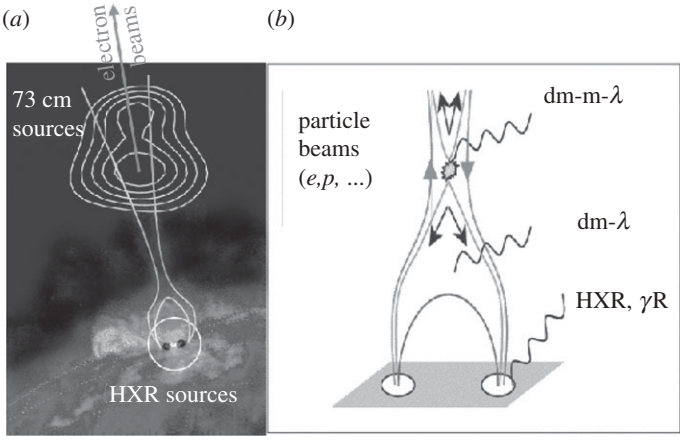

Figure 11. (*a*) Overlay of hard X-ray sources from RHESSI (black contours within the white circle) and radio sources from the the Nançay Radioheliograph (NRH; white contours) on an EUV image (SOHO/EIT) of the flaring active region (adapted from Vilmer *et al.* [58]). The grey lines are a schematic of a plausible magnetic configuration showing both closed lines and open lines to the high corona (and potentially the interplanetary medium) in which radio emissions from decimetric to kilometric emissions can be produced. (*b*) Scenario for flare-related particle acceleration derived from these observations.

electrons of a few tens of keV injected upwards and downwards in the corona from the acceleration site. The electron beams propagate along the coronal magnetic field lines and produce coherent emissions at the local plasma frequency or at its harmonic. The emitted radio bursts exhibit characteristic frequency drifts from high to low frequencies when the beam propagates upwards in the corona (i.e. opposite to the ambient density gradient). In some events, the electron beams may propagate from the acceleration site in the low corona to the interplanetary medium. Associated radio emissions are then observed in a whole frequency range going from several hundreds of megahertz (emission originating close to the electron acceleration region) to a few megahertz or less (few megahertz emission typically originates at heights of several 10^7 km in the solar atmosphere (0.1 AU)). Figure 11*b* (adapted from [59]) shows a simple cartoon illustrating the location of the particle acceleration site in the corona with respect to the locations of the radio and HXR emitting sites. The upward field lines may also provide access in some cases to heliospheric field lines (see §5*b*). Figure 11*a* shows the locations of the HXR and radio sources observed for a specific flare [58]. For this event, a very close correspondence between the change in the pattern of the HXR source in the 25–40 keV range and the pattern of the radio source at the highest imaged frequency (410 MHz–73 cm) is observed. This strongly supports the idea of a common acceleration/injection site for emitting electrons located in a region such that shown in figure 11. The electron acceleration height can also be deduced from the combined analysis of observations and analytical/numerical models of electron transport in the corona [60]. Figure 12 shows the time evolution of the HXR emission together with the radio spectrum from 550 to 1 MHz for the flare discussed in figure 11*a*. The link between HXR producing electrons and electron beams propagating in the corona towards the high corona or the interplanetary medium is, however, not always

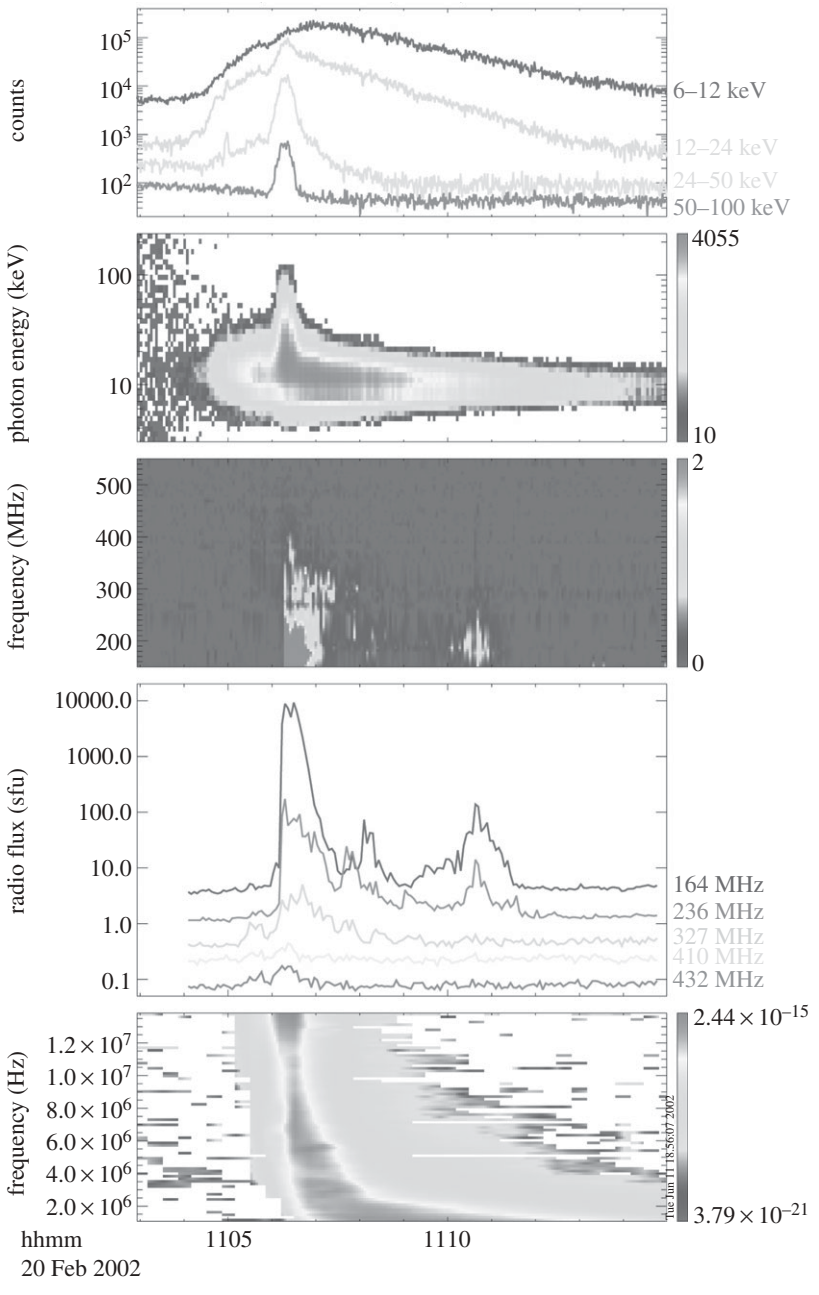

Figure 12. Multi-frequency observations of the radiative signatures of energetic electrons from the chromosphere to the high corona. From top to bottom: time profiles of hard X-ray count-rates from RHESSI, dynamic hard X-ray spectrum from RHESSI, dynamic dm-m radio spectrum from PHOENIX-2, selected dm-m time histories (NRH), dynamic deka-hectometre spectrum from Wind/Waves (from Vilmer *et al.* [58]).

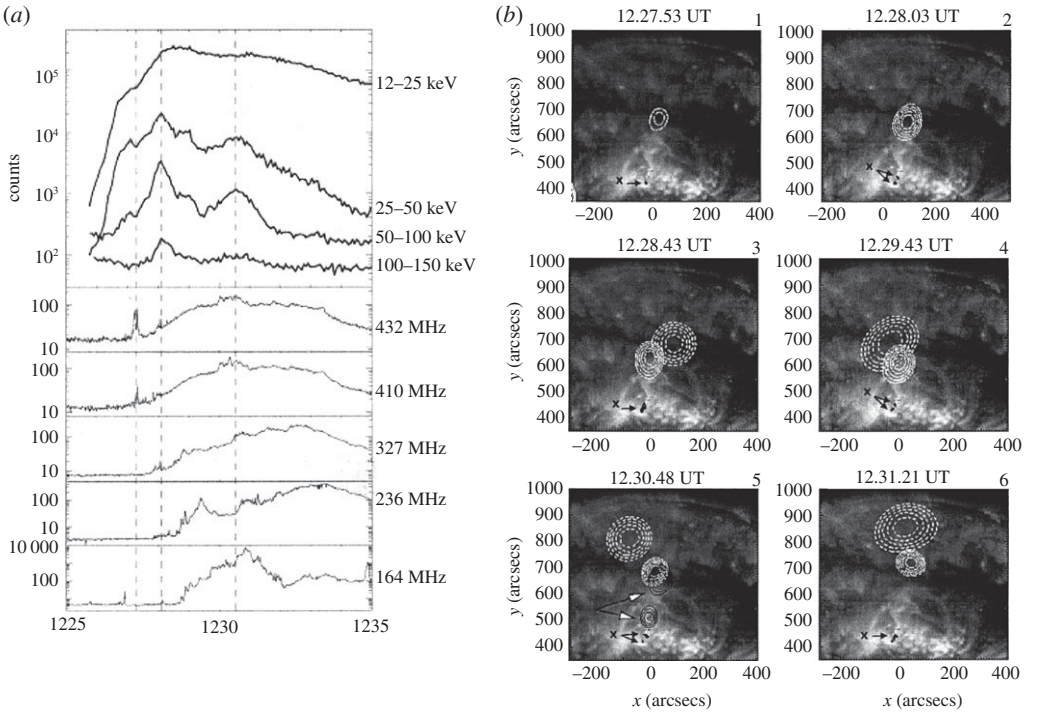

Figure 13. (*a*) Time evolution of the X-ray count-rates in four energy bands (top) and time evolution of the radio flux density observed in the flare region by the NRH (bottom). The dashed vertical lines indicate the first radio 432 MHz burst at 12.27.20 UT and the two main HXR peaks above 50 keV around 12.28 UT and after 12.30 UT. (*b*) RHESSI isocontours (thick black) and NRH contours at 327 MHz (dashed-dotted white) and 164 MHz (dotted white; 75%, 80%, 85%, 90%, 95% of the maximum for all contours) observed at different times. Note that the 164 MHz emission appears later in the flare (from image 3). The two components at 432 MHz (indicated by arrows) are overlaid for comparison (black contours) in image 5. The RHESSI and NRH contours are overlaid on the EIT image. The RHESSI contours are obtained in the 40–65 keV range and are indicated by black arrows (from Vilmer *et al.* [61]).

as simple as suggested by figure 12. Indeed, figure 13 illustrates an example in which the link between HXR emissions and radio decimetric/metric emissions clearly changes on a time scale of a few minutes. While the first HXR peak in the 50–100 keV range is not associated with strong radio emissions below 400 MHz, the second one is associated with intense decimetric/metric (and decametric) emissions. At the time of the second peak, the hard X-ray emission is found to originate from a slightly different position in the active region and is associated with the appearance of new radio components at all frequencies with positions further away from the active region (figure 13*b*). Injection of energetic electrons in different magnetic structures and in larger scale (more than 10^5 km) structures are thus involved at the time of the second HXR peak. This second HXR peak also corresponds to the time of extension of strong radio emission below 14 MHz. The radio sources at different frequencies in the second peak thus trace the electron beam injection towards the high corona and the potential link to the interplanetary medium.

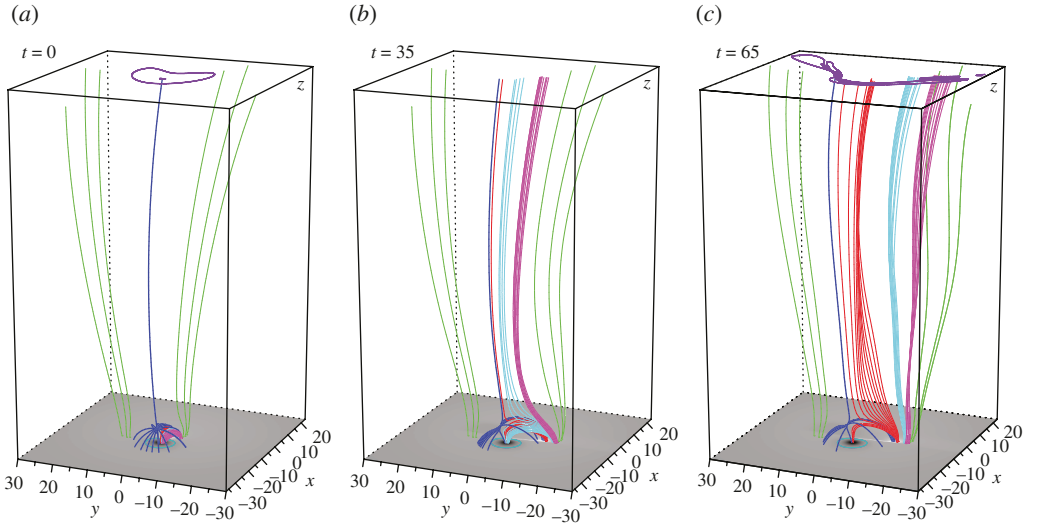

Figure 14. Evolution of selected magnetic field lines. The dark blue lines are the spine and fan field lines passing through the null point. The green field lines represent the open diverging magnetic field. The other coloured field lines are plotted with fixed footpoints in the prescribed photospheric flow. The distribution of the vertical photospheric magnetic field Bz ($z = 0$) is coded in grey scale. (a) Initial ($t = 0$) magnetic configuration: the pink field lines are located below the fan surface in the inner connectivity domain. (b,c) $t = 35$ and 65: evolution of magnetic field lines in the outer connectivity domain (adapted from Masson *et al.* [62]).

(b) *Electron injection from the flare site to the interplanetary medium*

In the classical cartoon such as the one in figure 3*b*, there are no open field lines. However, for flare particles to escape into interplanetary space, they must have access to such lines. Radio observations (figures 11–13) show that electrons have access to field lines connecting at least the acceleration region to the low corona and, in some cases, even to the heliosphere. As shown in figure 13, the access to heliospheric lines may evolve during a flare. The progressive access of particles to open field lines could occur through the process of interchange reconnection in which newly emerging flux tubes can reconnect with previously open lines. Upward-moving electrons accelerated in this new reconnection site could then escape along newly opened field lines to the high corona and interplanetary medium. A new model based on slip-running reconnection has been proposed to explain how particles accelerated at a reconnection site and initially not magnetically connected to the Earth could later propagate along well-connected open field lines [62]. A three-dimensional magnetohydrodynamics (MHD) simulation is used to show how, in a configuration with a coronal null point which has a closed fan surface and an open outer spine, the field lines initially rooted in the closed connectivity domain and driven by slow photospheric motions (figure 14*a*) may reconnect at the null point and jump to the open magnetic domain. This is similar to the standard interchange mode in the two-dimensional configuration (e.g. [63]), but in the three-dimensional configuration, the reconnected open field lines located in the vicinity of the outer spine keep reconnecting continuously. This leads to an

apparent slipping motion of these field lines (figure 14*c*), leading to the formation of an extended narrow magnetic flux tube at high altitudes. Because of the slip-running reconnection, the energetic particles can then be successively injected along continuously reconnecting field lines that are connected farther and farther from the spine. Such a model based on slip-running reconnection could improve our understanding of particle escape in open magnetic field lines in the high corona and the interplanetary medium. In the future, particle acceleration in the corona and escape in the interplanetary medium will be one of the objectives of the Solar Orbiter mission.

6. Energetic particles at the Sun and in the interplanetary medium

In addition to producing flare energetic particles responsible for many radiations, the Sun also emits charged particles and neutrons, which escape into the interplanetary medium and eventually reach the Earth's atmosphere. The solar energetic particle (SEP) events have been measured with energies up to 100 MeV by a fleet of spacecraft (ACE, SOHO, STEREO, Ulysses, Wind, etc.). The more energetic protons (above 450 MeV) are measured by neutron monitors at Earth. SEP events were originally divided into two groups, referred to as 'impulsive' and 'gradual' events, and this classification was commonly accepted until the launch of the ACE in 1997. In the two-class paradigm for SEP events proposed by Reames [64,65], the flare process accounts for the acceleration of the impulsive events. On the other hand, for the long duration gradual events, the acceleration is dominated by CME-driven coronal and interplanetary shocks (not flares). Several *in situ* measurements of the composition and of the charge states of ions, more particularly from ACE [66], have indicated that this view is probably oversimplified. These observations show indeed that gradual SEP events are accelerated not only from the solar wind plasma but also from an additional seed population (for a review, see Mewaldt *et al.* [67]). On the other hand, the ability of shocks to accelerate rapidly up to GeV energies coronal and solar wind particles has been questioned. In conclusion, there is now a general agreement that the two-class paradigm was too simplified and that gradual SEP events include particles that originate from flares and from CMEs in different ways: particles can be accelerated by CME-driven shocks but also in the reconnection sites of flares and CMEs.

The occurrence of SEPs has been shown recently to be strongly associated with a specific spectral evolution of the solar HXR spectrum (hardening of the photon and thus of the electron spectrum in the course of the flare), therefore suggesting a direct connection between the acceleration processes of interacting and escaping particles. This effect had been noted originally by Kiplinger [68] for around 20 SEP events and has been re-examined recently with RHESSI. Grayson *et al.* [69] analysed all the GOES X and M-class flares well observed with RHESSI and magnetically well-connected with the Earth (W30–W90). They found that 12 of the 18 flares exhibiting a spectral hardening of the X-ray (and electron) spectrum in the development of the flare were associated with a SEP event, whereas none of the 19 flares without this specific spectral hardening behaviour was associated with a SEP event. This shows a statistically significant dependence of the spectral evolution of the electrons interacting at the Sun and of

the occurrence of a strong energetic proton event in the interplanetary medium. This kind of observation does not support a scenario in which escaping energetic particles would be accelerated at the shock front of the CME but rather supports a more direct link with the acceleration of particles at the flare site. Figure 7*b* shows such an evolution of the hard X-ray spectrum for the flare of 20 January 2005 which was associated with one of the largest relativistic proton events measured so far with neutron monitors [70,71]. For this event, it was found by Masson *et al.* [71] that the first release of relativistic protons at the Sun corresponds to the time of the production at the Sun of more than 300 MeV protons revealed by their very high-energy γ-ray radiation observed with CORONAS-F/SONG. This shows an even closer link between the acceleration of very energetic ions at the Sun and the injection of relativistic protons into the interplanetary medium. The mechanisms producing such high-energy particles in the flare sites are however far from being understood.

7. Acceleration mechanisms

Particle acceleration in solar flares is a very challenging issue, given the constraints imposed by the observations reviewed earlier. The acceleration model(s) needs to explain the mechanism(s) that transfers more than 50 per cent of magnetic energy to large numbers of energetic electrons and ions, which are also able to accelerate electrons to more than 100 MeV and ions to GeV energies on very short time scales (seconds to minutes). Many reviews have dealt with this problem of particle acceleration [72]. The most recent review by Zharkova *et al.* [47] provides extensive details on basic theoretical concepts as well as on the new developments in the field, such as particle acceleration in three-dimensional magnetic field configurations and stochastic acceleration in a turbulent environment. At a fundamental level, particles are accelerated by an electric field. Differences in the structure and temporal evolution of the accelerating electric field and its relationship to large-scale magnetic structures allow particle acceleration models to be classified in terms of several basic scenarios. The acceleration mechanisms studied in great detail in the field of solar physics (but also for astrophysical plasmas) are shock waves (e.g. [73]), stochastic acceleration by high-frequency waves (see the review by Miller *et al.* [72]) and DC electric fields [39,74]. In the complex magnetic environment of solar flares, multiple acceleration mechanisms most probably operate simultaneously or successively (for a review, see [46]). In the 1990s and before the RHESSI era, a lot of emphasis was given to the study of shock wave acceleration (for flare energetic particles) and stochastic acceleration by waves; recently, though, more emphasis has been given to acceleration processes that are likely to occur in regions of magnetic reconnection. Reconnection can also result in the formation of shocks that can also accelerate particles in fast reconnection outflows or in the generation of turbulence also leading to particle acceleration. Acceleration by large-scale Alfvén waves launched in the primary reconnection site has also been recently considered [75]. Even if the past decade has seen significant progress in the development of particle acceleration models in flares, a major challenge that still needs to be addressed is the effect (feedback) of the accelerated particles on the acceleration structures themselves (current sheets, shocks, etc.). The link

between the magnetic topology that can be derived from observations and the characteristics of the accelerated particles is also still far from being understood and predictable. To be able to link what happens at the large scales of coronal magnetic structures and at the small kinetic scales where particles are accelerated also remains a challenging task to achieve.

Some developments in the field of particle acceleration in reconnecting current sheets were achieved in the last few years: acceleration in super-Dreicer electric field in a simple three-dimensional magnetic topology [76,77] and particle acceleration in three-dimensional spine and fan reconnection [78,79]. Several approaches have been considered (test particle and particle in cell simulations). In the test particle approach developed in Zharkova & Gordovskyy [76], protons and electrons are ejected from the reconnecting current sheet with a power-law distribution with a spectral index and a low energy cut-off that depend on the magnitude of the guiding magnetic field (parallel to the electric field) in the current sheet. Depending on the magnitude of this guiding field, protons and electrons can be ejected asymmetrically from the sheet (this could be one of the reasons for the displacements of X-ray and γ-ray sources; see §3*d*). Proton acceleration during three-dimensional spine and fan reconnection has been considered by Dalla & Browning [78,79] (for details of three-dimensional reconnection, see [80,81]). It is found (figure 15*a*) that a significant fraction of protons can be accelerated in these processes to energies above 100 keV. In both configurations, a power-law spectrum is obtained for the accelerated particles, but in the case of spine reconnection, a larger population of higher energy protons (the ones that can produce γ-ray line emissions) is produced. This shows that in such models, ions are not in all cases accelerated to the high energies which can produce γ-ray emission. Acceleration by many current sheets as discussed later may be the necessary ingredient to explain how protons can reach high enough energies to produce γ-rays.

A lot of effort has been recently devoted to models of particle acceleration involving multiple acceleration sites. Particle acceleration has been investigated by using an ensemble of shock waves [84], MHD simulations combined with relativistic test particle codes [82,85,86] or cellular automaton (CA) models based on the concept of self-organized criticality that can mimic the complex evolution of the magnetic energy released in a solar flare. As an illustration, Turkmani *et al.* [82] looked at particle acceleration in a stressed coronal magnetic configuration derived from the MHD simulations of Galsgaard & Nordlund [87]. Test particles are injected in the coronal structure whose state is fixed at a given time and their motions are simulated in the fields associated with the multiple current sheets which have been created. The acceleration of particles to relativistic energies is found to be very fast (even for high-energy protons) and efficient. The resulting distribution function of accelerated particles has a clear double power-law structure with a thermal component at low energies (figure 15*b*). CA models are also used to study electron and ion acceleration. Particle acceleration is linked to the presence of randomly placed localized electric fields (current sheets) simulated by the energy release process in the CA model. At each encounter with a current sheet, particles randomly gain or lose energy. Dauphin *et al.* [83] considered the dependence of the particle energy gain on the current sheet magnetic configuration (essentially the magnitude of the guiding field in the current sheet). In such a case, electrons, protons and heavier ions

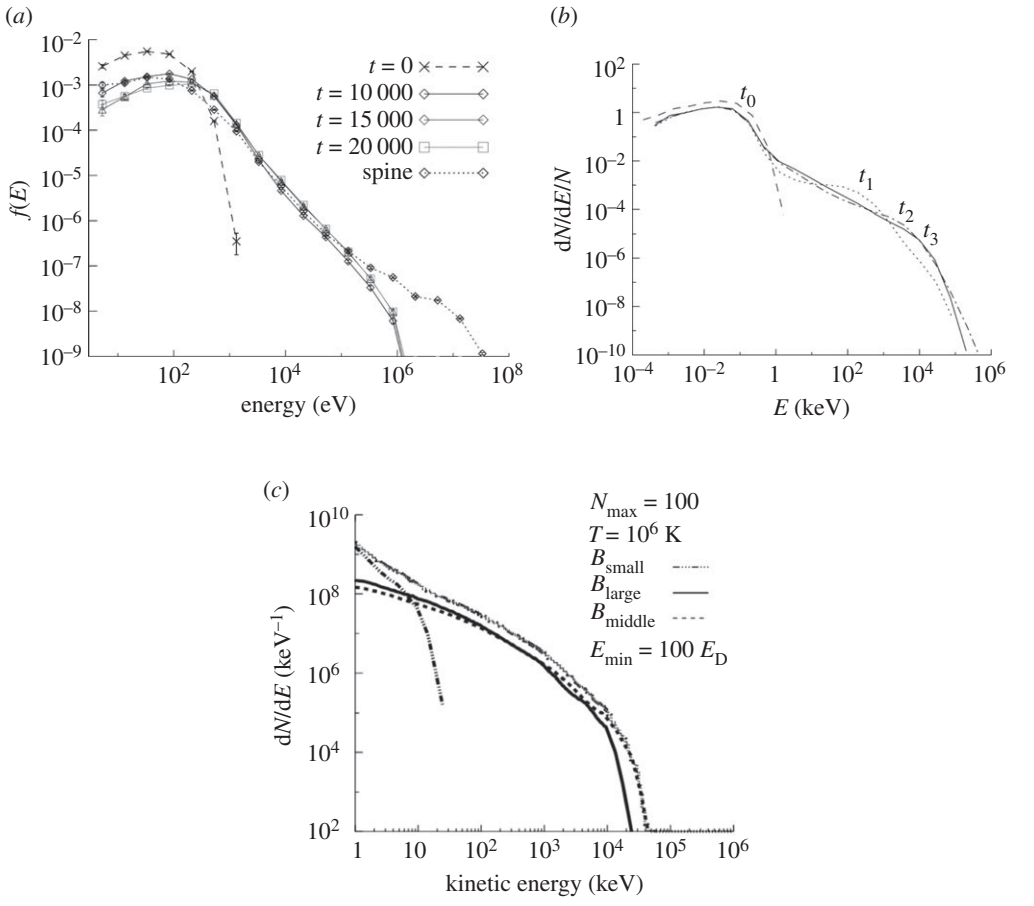

Figure 15. (*a*) Energy spectra of accelerated protons in fan reconnection at successive times, showing evolution towards a steady state. The final energy spectrum for spine reconnection is also shown for comparison (from Dalla & Browning [79]). (*b*) Energy spectra of accelerated protons in the case of particle acceleration in stochastic current sheets derived from stressed coronal active regions (from Turkmani *et al.* [82]). (*c*) Electron energy distributions resulting from acceleration in many current sheets. The dashed-dotted line corresponds to the case of small guiding fields in the current sheets, the dashed line corresponds to the case of moderate guiding fields and the black line corresponds to the case of strong guiding fields (from Dauphin *et al.* [83]).

may have different energy gain in the current sheet which results in different final energy spectra. Depending on the configurations, the model can either reproduce events with major electron acceleration or events with significant γ-ray line emissions. The energy contained in electrons above 20 keV and protons above 1 MeV accelerated in a total volume (containing distributed reconnecting current sheets) of $100''^3$ is in agreement with what is deduced from the observations of HXR/GR flares. The large acceleration efficiency found in this paper is attributed to the values of the electric fields in the current sheets (super-Dreicer fields). Such values allow a large fraction of the initial Maxwellian particle distribution to be brought to the non-thermal energy range. Flat particle spectra (electron spectra shown in figure 15*c*) are obtained in the energy range around a few keV to several

hundreds of keV followed by a strong softening of the spectra at higher energy. It should be noted that such a flat spectrum is characteristic of most models invoking multiple particle acceleration sites (see also [82]). As a consequence, the X-ray spectra predicted in these models are usually too flat with respect to the observed ones.

8. Conclusions

The last decade has seen significant progress in the field of solar flares observed at high energies and of the associated production of energetic particles. The images obtained in the X-ray and γ-ray energy range with RHESSI have confirmed the location of the particle acceleration site in the low corona with observations of several coronal hard X-ray sources (up to several hundreds of keV in a large flare). The imaging-spectroscopy capability of RHESSI has also allowed the X-ray spectrum (and then the electron spectrum) to be measured in the coronal source in which acceleration presumably takes place. The first images of flares in the γ-ray line domain led to unexpected results in showing that electron and ion acceleration sites can be significantly displaced at the solar surface. The number of flares for which all these new imaging observations were performed is however limited, given the sensitivity and the dynamic range over which imaging can be performed with RHESSI. A lot of progress in the imaging techniques is still needed to be able to detect more systematically the coronal sources and to image both electron and ion interaction sites so as to better constrain the acceleration and/or transport processes of both electrons and ions.

The possibility to measure hard X-ray spectra at high spectral resolution has allowed the observed photon spectra to be inverted to get the electron spectra in the emission site. This was, however, carried out for a limited number of events, and the aim would be to achieve these inversions on spatially resolved spectra to better constrain both the electron spectrum in the acceleration region and the effects of the transport on the electron spectra. Spectra with high spectral resolution were obtained with RHESSI and INTEGRAL, allowing the shapes of the γ-ray lines to be studied for some events. This provides some information on the angular distribution of the accelerated particles, and, once combined with the spectral analysis on the complete γ-ray spectrum, constraints on the relative abundances of accelerated helium to accelerated protons. Even if such an analysis is performed nowadays on just a few events, it clearly shows how observations with higher sensitivity would improve our knowledge on ion acceleration in solar flares. The observation of a rough correlation between X-ray emissions above 300 keV and the γ-ray fluence in the 2.2 MeV line suggests that all the flares which produce significant emissions from electrons at high energies also produce significant emission in the γ-ray line domain. This strongly supports the fact that electron and ion acceleration processes are linked in solar flares, even if there are variations in the accelerated-electron-to-proton ratio from flare to flare or even in the course of a flare. The correlation between relativistic electrons and ions is, however, better than the one between ions and sub-relativistic electrons. All these observations bring strong constraints to the acceleration processes which should operate in the context of solar flares.

The production of energetic particles in solar flares is still a challenging issue. In particular, models must explain how 50 per cent of the magnetic free energy can be converted to fast particles and how particles can be accelerated to the very high energies that are required to explain, for example, the observations of pion decay radiation, the production of neutrons as well as some sub-millimetre observations that were not discussed in this review. A lot of work has been devoted in the past decade to particle acceleration processes in multiple acceleration sites as well as to the study of particle acceleration in reconnecting current sheets based on three-dimensional magnetic configurations. The link between the magnetic configuration and the acceleration processes is, however, far from being presently understood.

The relationship between energetic particles interacting at the Sun, propagating in the corona and escaping in the interplanetary medium is also a domain in which many results have been obtained in the last decade. Combining radio and hard X-ray observations may provide information on the electron acceleration sites and also allow one to understand how electrons (and protons) have access to open magnetic structures. The link between specific spectral evolution of HXR events and the association with SEPs has been (re)confirmed from recent observations. The release of relativistic particles in the interplanetary medium has also been found for many events to be associated with the hardest phase of the γ-ray flare. The link between energetic particles at the Sun and in the interplanetary medium will, however, still remain a very active domain in the next decade in the context of the Solar Orbiter mission.

This study was supported by the European Community Framework Programme 7, 'High energy solar physics data in Europe (HESPE)', grant agreement no. 263086. The author expresses her thanks to the referees and the editor for their careful reading of the manuscript and their wise comments.

References

1 Carrington, R. C. 1859 Description of a singular appearance seen in the sun on September 1, 1859. *Mon. Not. R. Astron. Soc.* **20**, 13–15.
2 Sturrock, P. A. 1980 Solar flares: a monograph from SKYLAB solar workshop II.
3 Emslie, A. G., Dennis, B. R., Hudson, H. & Lin, R. P. 2011 High-energy aspects of solar flares: a RHESSI-inspired monograph. *Space Sci. Rev.* **159**, 1–2. (doi:10.1007/s11214-011-9815-7)
4 Emslie, A. G. *et al.* 2004 Energy partition in two solar flare/CME events. *J. Geophys. Res.* (*Space Phys.*) **109**, 10104. (doi:10.1029/2004JA010571)
5 Fletcher, L. *et al.* 2011 An observational overview of solar flares. *Space Sci. Rev.* **159**, 19–106. (doi:10.1007/s11214-010-9701-8)
6 Lin, R. P. *et al.* 2002 The Reuven Ramaty High-Energy Solar Spectroscopic Imager (RHESSI). *Sol. Phys.* **210**, 3–32. (doi:10.1023/A:1022428818870)
7 Lin, R. P. *et al.* 2003 RHESSI observations of particle acceleration and energy release in an intense solar gamma-ray line flare. *Astrophys. J. Lett.* **595**, L69–L76. (doi:10.1086/378932)
8 Brown, J. C. 1971 The deduction of energy spectra of non-thermal electrons in flares from the observed dynamic spectra of hard X-ray bursts. *Sol. Phys.* **18**, 489–502. (doi:10.1007/BF00149070)
9 Holman, G. D., Aschwanden, M. J., Aurass, H., Battaglia, M., Grigis, P. C., Kontar, E. P., Liu, W., Saint-Hilaire, P. & Zharkova, V. V. 2011 Implications of X-ray observations for electron acceleration and propagation in solar flares. *Space Sci. Rev.* **159**, 107–166. (doi:10.1007/s11214-010-9680-9)

10 Kontar, E. P. *et al.* 2011 Deducing electron properties from hard X-ray observations. *Space Sci. Rev.* **159**, 301–355. (doi:10.1007/s11214-011-9804-x)
11 Ramaty, R. 1986 Nuclear processes in solar flares. In *Physics of the sun*, vol. 2 (eds P. A. Sturrock, T. E. Holzer, D. M. Mihalas & R. K. Ulrich), pp. 291–323. Dordrecht, The Netherlands: Reidel Publishing.
12 Share, G. H. & Murphy, R. 2006 Gamma radiation from flare-accelerated particles impacting the sun. *Am. Geophys. Union Geophys. Monogr. Ser.* **165**, 177–179. (doi:10.1029/165GM17)
13 Vilmer, N., MacKinnon, A. L. & Hurford, G. J. 2011 Properties of energetic ions in the solar atmosphere from γ-ray and neutron observations. *Space Sci. Rev.* **159**, 167–224. (doi:10.1007/s11214-010-9728-x)
14 Chupp, E. L. & Ryan, J. M. 2009 High energy neutron and pion-decay gamma-ray emissions from solar flares. *Res. Astron. Astrophys.* **9**, 11–40. (doi:10.1088/1674-4527/9/1/003)
15 Vedrenne, G. *et al.* 2003 SPI: the spectrometer aboard INTEGRAL. *Astron. Astrophys.* **411**, L63–L70. (doi:10.1051/0004-6361:20031482)
16 Temmer, M., Veronig, A. M., Vršnak, B. & Miklenic, C. 2007 Energy release rates along Hα flare ribbons and the location of hard X-ray sources. *Astrophys. J. Lett.* **654**, 665–674. (doi:10.1086/509634)
17 Masuda, S., Kosugi, T., Sakao, T. & Sato, J. 1998 Summary of coronal hard X-ray sources observed with Yohkoh/HXT. In *Observational plasma astrophysics* (eds T. Watanabe & T. Kosugi), pp. 259–268. Dordrecht, The Netherlands: Kluwer Academic.
18 Bogachev, S. A., Somov, B. V., Kosugi, T. & Sakao, T. 2005 The motions of the hard X-ray sources in solar flares: images and statistics. *Astrophys. J. Lett.* **630**, 561–572. (doi:10.1086/431918)
19 Démoulin, P., Bagala, L. G., Mandrini, C. H., Henoux, J. C. & Rovira, M. G. 1997 Quasi-separatrix layers in solar flares. II. Observed magnetic configurations. *Astron. Astrophys.* **325**, 305–317.
20 Metcalf, T. R., Alexander, D., Hudson, H. S. & Longcope, D. W. 2003 TRACE and Yohkoh observations of a white-light flare. *Astrophys. J. Lett.* **595**, 483–492. (doi:10.1086/377217)
21 des Jardins, A., Canfield, R., Longcope, D., Fordyce, C. & Waitukaitis, S. 2009 Reconnection in three dimensions: the role of spines in three eruptive flares. *Astrophys. J. Lett.* **693**, 1628–1636. (doi:10.1088/0004-637X/693/2/1628)
22 Pontin, D. I. 2012 Theory of magnetic reconnection in solar and astrophysical plasmas. *Phil. Trans. R. Soc. A* **370**, 3169–3192. (doi:10.1098/rsta.2011.0501)
23 Sui, L. & Holman, G. D. 2003 Evidence for the formation of a large-scale current sheet in a solar flare. *Astrophys. J. Lett.* **596**, L251–L254. (doi:10.1086/379343)
24 Aschwanden, M. J., Schwartz, R. A. & Dennis, B. R. 1998 Deconvolution of directly precipitating and trap-precipitating electrons in solar flare hard X-rays. II. Compton gamma ray observatory data analysis. *Astrophys. J. Lett.* **502**, 468. (doi:10.1086/305891)
25 Brown, J. C., Turkmani, R., Kontar, E. P., MacKinnon, A. L. & Vlahos, L. 2009 Local re-acceleration and a modified thick target model of solar flare electrons. *Astron. Astrophys.* **508**, 993–1000. (doi:10.1051/0004-6361/200913145)
26 Brown, J. C., Conway A. J. & Aschwanden, M. J. 1998 The electron injection function and energy-dependent delays in thick-target hard X-rays. *Astrophys. J. Lett.* **509**, 911–917. (doi:10.1086/306522)
27 Wang, T., Sui, L. & Qiu, J. 2007 Direct observation of high-speed plasma outflows produced by magnetic reconnection in solar impulsive events. *Astrophys. J. Lett.* **661**, L207–L210. (doi:10.1086/519004)
28 Krucker, S. *et al.* 2008 Hard X-ray emission from the solar corona. *Astron. Astrophys. Rev.* **16**, 155–208. (doi:10.1007/s00159-008-0014-9)
29 Krucker, S., Hurford, G. J., MacKinnon, A. L., Shih, A. Y., & Lin, R. P. 2008 Coronal γ-ray bremsstrahlung from solar flare-accelerated electrons. *Astrophys. J. Lett.* **678**, L63–L66. (doi:10.1086/588381)
30 Saldanha, R., Krucker, S. & Lin, R. P. 2008 Hard X-ray spectral evolution and production of solar energetic particle events during the January 2005 X-class flares. *Astrophys. J. Lett.* **673**, 1169–1173. (doi:10.1086/524929)

31 Vilmer, N., Trottet, G., Barat, C., Schwartz, R. A., Enome, S., Kuznetsov, A., Sunyaev, R. & Terekhov, O. 1999 Hard X-ray and gamma-ray observations of an electron dominated event associated with an occulted solar flare. *Astron. Astrophys.* **342**, 575–582.
32 Frost, K. J. & Dennis, B. R. 1971 Evidence from hard X-rays for two-stage particle acceleration in a solar flare. *Astrophys. J. Lett.* **165**, 655–659. (doi:10.1086/150932)
33 Vestrand, W. T. & Forrest, D. J. 1993 Evidence for a spatially extended component of gamma rays from solar flares. *Astrophys. J. Lett.* **409**, L69–L72. (doi:10.1086/186862)
34 Barat, C., Trottet, G., Vilmer, N., Dezalay, J.-P., Talon, R., Sunyaev, R., Terekhov, O. & Kuznetsov, A. 1994 Evidence for intense coronal prompt gamma-ray line emission from a solar flare. *Astrophys. J. Lett.* **425**, L109–L112. (doi:10.1086/187322)
35 Hurford, G. J., Schwartz, R. A., Krucker, S., Lin, R. P., Smith, D. M. & Vilmer, N. 2003 First gamma-ray images of a solar flare. *Astrophys. J. Lett.* **595**, L77–L80. (doi:10.1086/378179)
36 Hurford, G. J., Krucker, S., Lin, R. P., Schwartz, R. A., Share, G. H. & Smith, D. M. 2006 Gamma-ray imaging of the 2003 October/November solar flares. *Astrophys. J. Lett.* **644**, L93–L96. (doi:10.1086/505329).
37 Emslie, A. G., Miller, J. A. & Brown, J. C. 2004 An explanation for the different locations of electron and ion acceleration in solar flares. *Astrophys. J. Lett.* **602**, L69–L72. (doi:10.1086/382350)
38 Dauphin, C. & Vilmer, N. 2007 Time delay between γ-ray lines and hard X-ray emissions during the 23 July 2002 solar flare interpreted by a trap plus precipitation model. *Astron. Astrophys.* **468**, 289–298. (doi:10.1051/0004-6361:20066247)
39 Litvinenko, Y. E. & Somov, B. V. 1993 Particle acceleration in reconnecting current sheets. *Sol. Phys.* **146**, 127–133. (doi:127-110.1007/BF0066217433)
40 Zharkova, V. V. & Gordovskyy, M. 2004 Particle acceleration asymmetry in a reconnecting nonneutral current sheet, *Astrophys. J.* **604**, 884–891. (doi:10.1086/381966)
41 Piana, M., Massone, A. M., Kontar, E. P., Emslie, A. G., Brown, J. C. & Schwartz, R. A. 2003 Regularized electron flux spectra in the 23 July 2002 solar flare. *Astrophys. J. Lett.* **595**, L127–L130. (doi:10.1086/378171)
42 Holman, G. D., Sui, L., Schwartz, R. A. & Emslie, A. G. 2003 Electron bremsstrahlung hard X-ray spectra, electron distributions, and energetics in the 2002 July 23 solar flare. *Astrophys. J. Lett.* **595**, L97–L101. (doi:10.1086/378488)
43 Kiener, J., Gros, M., Tatischeff, G. & Weidenspointner, G. 2006 Properties of the energetic particle distributions during the 28 October 2003 solar flare from INTEGRAL/SPI observations. *Astron. Astrophys.* **445**, 725–733. (doi:10.1051/0004-6361:20053665)
44 Massone, A. M., Emslie, A. G., Kontar, E. P., Piana, M., Prato, M. & Brown, J. C. 2004 Anisotropic bremsstrahlung emission and the form of regularized electron flux spectra in solar flares. *Astrophys. J. Lett.* **613**, 1233–1240. (doi:10.1086/423127)
45 Crosby, N. B., Aschwanden, M. J. & Dennis, B. R. 1993 Frequency distributions and correlations of solar X-ray flare parameters. *Sol. Phys.* **143**, 275–299. (doi:10.1007/BF00646488)
46 Vlahos, L., Krucker, S. & Cargill, P. 2009 The solar flare: a strongly turbulent particle accelerator. In *Turbulence in space plasmas* (eds P. Cargill & L. Vlahos). Lecture Notes in Physics, no. 778, pp. 157–221. Berlin, Germany: Springer.
47 Zharkova, V. V. *et al.* 2011 Recent advances in understanding particle acceleration processes in solar flares. *Space Sci. Rev.* **159**, 357–420. (doi:10.1007/s11214-011-9803-y)
48 Grigis, P. C. & Benz, A. O. 2004 The spectral evolution of impulsive solar X-ray flares. *Astron. Astrophys.* **426**, 1093–1101. (doi:10.1051/0004-6361:20041367)
49 Trottet, G., Vilmer, N., Barat, C., Benz, A., Magun, A., Kuznetsov, A., Sunyaev, R. & Terekhov, O. 1998 A multiwavelength analysis of an electron-dominated gamma-ray event associated with a disk solar flare. *Astron. Astrophys.* **334**, 1099–1111.
50 Ramaty, R., Mandzhavidze, N. & Kozlovsky, B. 1996 Solar atmospheric abundances from gamma ray spectroscopy. *Am. Inst. Phys. Conf. Ser.* **374**, 172–183. (doi:10.1063/1.50953)
51 Share, G. H. & Murphy, R. J. 1995 Gamma-ray measurements of flare-to-flare variations in ambient solar abundances. *Astrophys. J. Lett.* **452**, 933. (doi:10.1086/176360)
52 Ramaty, R., Mandzhavidze, N., Kozlovsky, B. & Murphy, R. J. 1995 Solar atmospheric abundances and energy content in flare accelerated ions from gamma-ray spectroscopy. *Astrophys. J. Lett.* **455**, L193–L196. (doi:10.1086/309841)

53 Shih, A. Y., Lin, R. P. & Smith, D. M. 2009 RHESSI observations of the proportional acceleration of relativistic >0.3 MeV electrons and >30 MeV protons in solar flares. *Astrophys. J. Lett.* **698**, L152–L157. (doi:10.1088/0004-637X/698/2/L152)

54 Ramaty, R. & Mandzhavidze, N. 2000 Gamma-rays from solar flares. In *Highly energetic physical processes and mechanisms for emission from astrophysical plasmas* (eds P. C. H. Martens, S. Tsuruta & M. A. Weber), p. 123. San Francisco, CA: Astronomical Society of the Pacific.

55 Forrest, D. J. 1983 Solar gamma-ray lines. In *Positron–electron pairs in astrophysics*, vol. 101 (eds M. L. Burns, A. K. Harding & R. Ramaty), pp. 3–14. New York, NY: American Institute of Physics.

56 Chupp, E. L. 1984 High-energy neutral radiations from the sun. *Annu. Rev. Astron. Astrophys.* **22**, 359–387. (doi:10.1146/annurev.aa.22.090184.002043)

57 Pick, M. & Vilmer, N. 2008 Sixty-five years of solar radioastronomy: flares, coronal mass ejections and Sun Earth connection. *Astron. Astrophys. Rev.* **16**, 1–153. (doi:10.1007/s00159-008-0013-x)

58 Vilmer, N., Krucker, S., Lin, R. P. & The Rhessi Team 2002 Hard X-ray and metric/decimetric radio observations of the 20 February 2002 solar flare. *Sol. Phys.* **210**, 261–272. (doi:10.1023/A:1022492414597)

59 Klein, K.-L. 2007 High-energy particles at and from the Sun. In *Proc. Annu. Meeting of the French Society of Astronomy and Astrophysics*, SF2A-2007 (eds J. Bouvier, A. Chalabaev & C. Charbonnel), p. 7.

60 Reid, H. A. S., Vilmer, N. & Kontar, E. P. 2011 Characteristics of the flare acceleration region derived from simultaneous hard X-ray and radio observations. *Astron. Astrophys.* **529**, A66. (doi:10.1051/0004-6361/201016181)

61 Vilmer, N., Krucker, S., Trottet, G. & Lin, R. P. 2003 Hard X-ray and metric/decimetric spatially resolved observations of the 10 April 2002 solar flare. *Adv. Space Res.* **32**, 2509–2515. (doi:10.1016/j.asr.2003.04.005)

62 Masson, S., Aulanier, G., Pariat, E. & Klein, K. 2012 Interchange slip-running reconnection and sweeping SEP beams. *Solar Phys.* **276**, 199–217. (doi:10.1007/s11207-011-9886-3)

63 Edmondson, J. K., Lynch, B. J., Antiochos, S. K., De Vore, C. R. & Zurbuchen, T. H. 2009 Reconnection-driven dynamics of coronal-hole boundaries. *Astrophys. J. Lett.* **707**, 1427–1437. (doi:10.1088/0004-637X/707/2/1427)

64 Reames, D. V. 1995 Coronal abundances determined from energetic particles. *Adv. Space Res.* **15**, 41–51. (doi:10.1016/0273-1177(94)00018-V)

65 Reames, D. V. 1999 Particle acceleration at the Sun and in the heliosphere. *Space Sci. Rev.* **90**, 413–491. (doi:10.1023/A:1005105831781)

66 Cohen, C. M. S., Mewaldt, R. A., Leske, R. A. Cummings, A. C., Stone, E. C., Wiedenbeck, M. E., Christian, E. R. & von Rosenvinge, T. T. 1999 New observations of heavy-ion-rich solar particle events from ACE. *Geophys. Res. Lett.* **26**, 2697–2700. (doi:10.1029/1999GL900560)

67 Mewaldt, R. A., Cohen, C. M. S. & Mason, G. M. 2006 The source material for large solar energetic particle events. *Am. Geophys. Union Geophys. Monogr. Ser.* **165**, 115–125. (doi:10.1029/165GM12)

68 Kiplinger, A. L. 1995 Comparative studies of hard X-ray spectral evolution in solar flares with high-energy proton events observed at earth. *Astrophys. J. Lett.* **453**, 973–986. (doi:10.1086/176457)

69 Grayson, J. A., Krucker, S. & Lin, R. P. 2009 A statistical study of spectral hardening in solar flares and related solar energetic particle events. *Astrophys. J. Lett.* **707**, 1588–1594. (doi:10.1088/0004-637X/707/2/1588)

70 Flueckiger, E. O., Buetikofer, R., Desorgher, L. & Moser, M. R. 2006 The role of GLEs in space weather. In *36th COSPAR Scientific Assembly*, vol. 36, p. 3042.

71 Masson, S., Klein, K.-L., Bütikofer, R., FlückigerE., Kurt, V., Yushkov, B. & Krucker, S. 2009 Acceleration of relativistic protons during the 20 January 2005 flare and CME. *Sol. Phys.* **257**, 305–322. (doi:10.1007/s11207-009-9377-y)

72 Miller, J. A., Cargill, P. J., Emslie, A. G., Holman, G. D., Dennis, B. R., LaRosa, T. N., Winglee, R. M., Benka, S. G. & Tsuneta, S. 1997 Critical issues for understanding particle acceleration in impulsive solar flares. *J. Geophys. Res.* **102**, 14 631–14 660. (doi:10.1029/97JA00976)

73 Ellison, D. C. & Ramaty, R. 1985 Shock acceleration of electrons and ions in solar flares. *Astrophys. J. Lett.* **298**, 400–408. (doi:10.1086/163623)
74 Benka, S. G. & Holman, G. D. 1994 A thermal/nonthermal model for solar hard X-ray bursts. *Astrophys. J. Lett.* **435**, 469–481. (doi:10.1086/174829)
75 Fletcher, L. & Hudson, H. S. 2008 Impulsive phase flare energy transport by large-scale Alfvén waves and the electron acceleration problem. *Astrophys. J. Lett.* **675**, 1645–1655. (doi:10.1086/527044)
76 Zharkova, V. V. & Gordovskyy, M. 2005 Energy spectra of particles accelerated in a reconnecting current sheet with the guiding magnetic field. *Mon. Not. R. Astron. Soc.* **356**, 1107–1116. (doi:10.1111/j.1365-2966.2004.08532.x)
77 Zharkova, V. V. & Agapitov, O. V. 2009 The effect of magnetic topology on particle acceleration in a three-dimensional reconnecting current sheet: a test-particle approach. *J. Plasma Phys.* **75**, 159–181. (doi:10.1017/S002237780800771X)
78 Dalla, S. & Browning, P. K. 2006 Jets of energetic particles generated by magnetic reconnection at a three-dimensional magnetic null. *Astrophys. J. Lett.* **640**, L99–L102. (doi:10.1086/503302)
79 Dalla, S. & Browning, P. K. 2008 Particle trajectories and acceleration during 3D fan reconnection. *Astron. Astrophys.* **491**, 289–295. (doi:10.1051/0004-6361:200809771)
80 Priest, E. R. & Titov, V. S. 1996 Magnetic reconnection at three-dimensional null points. *Phil. Trans. R. Soc. Lond. A* **354**, 2951–2992. (doi:10.1098/rsta.1996.0136)
81 Priest, E. R. & Pontin, D. I. 2009 Three-dimensional null point reconnection regimes. *Phys. Plasmas* **16**, 122101. (doi:10.1063/1.3257901)
82 Turkmani, R., Cargill, P. J., Galsgaard, K., Vlahos, L. & Isliker, H. 2006 Particle acceleration in stochastic current sheets in stressed coronal active regions. *Astron. Astrophys.* **449**, 749–757. (doi:10.1051/0004-6361:20053548)
83 Dauphin, C., Vilmer, N. & Anastasiadis, A. 2007 Particle acceleration and radiation in flaring complex solar active regions modeled by cellular automata. *Astron. Astrophys.* **468**, 273–288. (doi:10.1051/0004-6361:20065131)
84 Anastasiadis, A. & Vlahos, L. 1994 Particle acceleration in an evolving active region by an ensemble of shock waves. *Astrophys. J. Lett.* **428**, 819–826. (doi:10.1086/174290)
85 Dmitruk, P., Matthaeus, W. H., Seenu, N. & Brown, M. R. 2003 Test particle acceleration in three-dimensional magnetohydrodynamic turbulence. *Astrophys. J. Lett.* **597**, L81–L84. (doi:10.1086/379751)
86 Onofri, M., Isliker, H. & Vlahos, L. 2006 Stochastic acceleration in turbulent electric fields generated by 3D reconnection. *Phys. Rev. Lett.* **96**, 151102. (doi:10.1103/PhysRevLett.96.151102)
87 Galsgaard, K. & Nordlund, Å. 1996 Heating and activity of the solar corona 1. Boundary shearing of an initially homogeneous magnetic field. *J. Geophys. Res.* **1011**, 13 445–13 460. (doi:10.1029/96JA00428)